

# Relation between quantum illumination and quantum parameter estimation

Wei Zhong,<sup>1,\*</sup> Wen-Yi Zhu,<sup>1</sup> Yang Li,<sup>1</sup> Lan Zhou,<sup>2</sup> Ming-Ming Du,<sup>3</sup> and Yu-Bo Sheng<sup>3,†</sup>

<sup>1</sup>*Institute of Quantum Information and Technology,*

*Nanjing University of Posts and Telecommunications, Nanjing 210003, China*

<sup>2</sup>*School of Science, Nanjing University of Posts and Telecommunications, Nanjing 210003, China*

<sup>3</sup>*College of Electronic and Optical Engineering, Nanjing University of Posts and Telecommunications, Nanjing 210003, China*

Quantum illumination (QI) leverages entangled lights to detect the potential presence of low-reflective objects in a region surrounded by a thermal bath. Homologously, quantum parameter estimation utilizes non-classical probes to accurately estimate the value of the unknown parameter(s) of interest in a system. There appears to be a certain connection between these two areas. However, they are commonly studied using different figures of merit: signal-to-noise ratio and quantum Fisher information. In this study, we prove that the two measures are equivalent to QI in the limit of zero object reflectivity. We further demonstrate this equivalence by investigating QI protocols employing non-Gaussian states, which are obtained by de-Gaussifying the two-mode squeezed vacuum state with photon addition and photon subtraction. However, our analysis leads to a no-go result which demonstrates that de-Gaussification operations do not offer an advantage compared to the null case.

## I. INTRODUCTION

Quantum illumination (QI) is a promising protocol that can give better performance in target detection than the optimum classical illumination [1–4]. In this protocol, the signal light being sent to illuminate a low-reflective object embedded in a bright environment is entangled with an idler (also called ancilla in [1]) light, and a joint measurement is performed on the reflected and idler lights simultaneously to detect whether the target is there or not (see Fig. 1). The QI protocol was first proposed by Lloyd [1] and enjoys a rather counterintuitive result that the QI's advantage accrues despite the final state of the reflected and idler lights being not entangled [5, 6]. This disputes the common belief that entangled states are only useful in noiseless situations due to the fact that quantum entangled states are fragile and easily disrupted by ambient noises.

Inspired by this pioneer work [1], a large amount of theoretical [7–15] and experimental [16–19] works have been completed. Among the currently proposed QI protocols, one of the most notable is the protocol by Tan *et al.* [7], which utilizes the two-mode squeezed vacuum (TMSV) state and achieves a gain up to 6 dB in the error probability exponent over coherent state with the same signal intensity. Recently, Bradshaw *et al.* strictly proved that the TMSV state is the optimal continuous-variable probe for QI in the limit of zero object reflectivity [20]. However, such a quantum-enhanced gain would hardly be achieved in experiments due to the difficulty in implementing the required joint measurement as it necessitates a quantum Schur transform [21]. In general, it is more experimentally friendly to implement a measurement which is based on local operations and classical communication protocol. Under the local measurement strategy, the

superiority of QI was also demonstrated with a gain in signal-to-noise ratio (SNR) up to 3 dB [9], which is half of what can be reaped with global measurements [7, 11].

More recently, Sanz *et al.* mapped the QI problem onto a quantum parameter estimation problem to estimate the reflectivity parameter of the object and demonstrated that using TMSV states yields an advantage up to 3 dB in quantum Fisher information (QFI) over coherent states [22]. This result is in agreement with that in terms of SNR [9], in the sense that there must be some connection between the SNR and the QFI. However, they were often considered separately [9, 10, 16, 22, 23], and no direct link between the two measures has yet been established. Although some attention has been devoted to this problem, it has been treated in a simplified manner by defining them as figures of merit for target detection and target sensitivity, respectively [14]. In this study, we tackle this issue by establishing an exact equivalence relationship between the SNR and the QFI in the QI setting. This equivalence reveals a clear operation meaning behind these two measures, helping to identifying the optimal measurement for saturating the ultimate bound on error probability with a local measurement strategy.

Moreover, we apply the aforementioned equivalence relationship to identify the optimal measurement for the QI protocols that employ two kinds of entangled states: multi-photon-added-TMSV (MPA-TMSV) and multi-photon-subtracted-TMSV (MPS-TMSV) states. These states are amongst the simplest non-Gaussian states that are experimentally available from the TMSV state by applying photon-addition and photon-subtraction operations. There are many works on the implementation of photon addition and photon subtraction in various research areas, including entanglement enhancement [24–32], entanglement distillation [26, 33–35], quantum teleportation [36–41], quantum phase estimation [42–45] as well as QI [46, 47]. As the result reported in [46, 47], photon addition and photon subtraction have a high relative advantage over not using them in target detection [46, 47]. However, our analysis gives a no-go result that

---

\* zhongwei1118@gmail.com

† shengyb@njupt.edu.cn

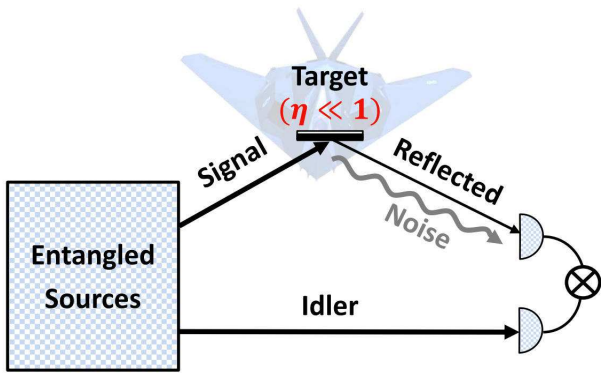


Figure 1. (Color online) Schematic representation of the concept of quantum illumination.

challenges this result.

This paper is structured as follows. In Sec. II, we briefly introduce the theoretical framework of QI and the two measures: SNR and QFI. We then present our main result by establishing an exact equivalence relationship between the QFI and the SNR. In Sec. III, we analytically derive the QFI expressions for the QI protocols that use MPA-TMSV and MPS-TMSV states as input states and identify the optimal measurement to saturate the QFI predicted bound of these protocols. In Sec. IV, a further discussion is centered on whether photon addition and photon subtraction are helpful for QI. Meanwhile, we provide a valuable insight in helping us understand our results. Finally, we present our conclusions in Sec. V.

## II. QUANTUM ILLUMINATION FORMALISM

### A. Quantum illumination

Quantum illumination aims to detect a low-reflectivity object suspected to be present in a region embedded in a thermal bath (see Fig. 1). A QI protocol involves creating a two-mode entangled light, with the signal mode directed towards the target region, while the idler mode is retained. The idler light is then measured with the reflected light from the target region simultaneously. The outcomes of measurement are then processed to confirm whether the object is present or not.

To formulate the above QI problem, the low-reflective object is modeled by a beam splitter described by the unitary transformation as

$$U(\eta) = \exp\left[\eta\left(a_S^\dagger b - a_S b^\dagger\right)\right], \quad (1)$$

where  $a_S$  and  $b$  are the annihilation operators for the signal and environment modes, respectively [22, 48]. The reflectivity of the object is then given by  $R = \sin^2 \eta \sim \eta^2$  under the assumption of  $\eta \ll 1$ . The bath state is

represented by

$$\rho_B = \sum_{n=0}^{\infty} \varrho_n |n\rangle_B \langle n|, \quad (2)$$

where  $\varrho_n = N_B^n / (N_B + 1)^{n+1}$  is the thermal distribution with an average photon number  $N_B$ . Denoting the initially prepared signal-idler mode state by  $\rho_{SI}$ , the final state to be detected, after evolving under  $U(\eta)$  and tracing out over the bath mode, is given by

$$\rho_{RI}^{(1)} = \text{Tr}_B[U(\eta) \rho_{SI} \otimes \rho_B U^\dagger(\eta)]. \quad (3)$$

This state represents the reduced density matrix with respect to the reflected and idler modes when the object is present. When  $\eta=0$ , which corresponds to the absence of the object, the final state becomes

$$\rho_{RI}^{(0)} = \rho_I \otimes \rho_B, \quad (4)$$

where  $\rho_I = \text{Tr}_B(\rho_{SI})$ . For simplicity we below use notations:  $\rho_0 \equiv \rho_{RI}^{(0)}$  and  $\rho_1 \equiv \rho_{RI}^{(1)}$ .

One insight from the above formulation is that the problem of determining whether the object is present or not is inherently related to the problem of discriminating between the two detected states,  $\rho_0$  and  $\rho_1$ . In other words, the QI problem can be viewed as a state discrimination problem [49]. On the other hand, the variation between  $\rho_0$  and  $\rho_1$  is infinitesimal due to the small object reflectivity amplitude  $\eta$ . It turns out that the task of distinguishing between  $\rho_0$  and  $\rho_1$  can be mapped to a task of estimating parameter  $\eta$ , namely the QI problem can be also viewed as a parameter estimation problem [50]. Based on this insightful understanding, two figures of merit were thus raised for QI: SNR [9, 15] and QFI [22]. Intuitively, there should be a close connection between the two measures. However, no such connection has been yet established. Below, we aim to solve it.

### B. Signal-to-noise ratio

Discriminating between  $\rho_0$  and  $\rho_1$ , as described above, is a typical binary hypothesis testing problem. In hypothesis testing terminology,  $\rho_0$  corresponds to the null hypothesis  $H_0$  of the absence of the object, and  $\rho_1$  to the alternative hypothesis  $H_1$  of the presence of the object. Here, we assign equal prior probability to both null and alternative hypotheses (i.e.,  $\pi_0 = \pi_1 = 1/2$ ), under the assumption of having no prior knowledge of the object.

An effective discrimination protocol generally relies on the repeated measurements with identical samples. A multitude of identical states for the two hypotheses can be presented in the tensor product form  $\rho_0^{\otimes M}$  and  $\rho_1^{\otimes M}$ , where  $M$  denotes the number of samples. To make a reliable discrimination, the number of samples is assumed to be sufficient large, i.e.,  $M \gg 1$ . This assumption is reasonable in realistic scenarios, such as continuous-wave

spontaneous parametric down-conversion, where each  $T$ -sec-long pulse produces  $M = WT \gg 1$  signal-idler mode pairs and  $W$  is the phase-matching bandwidth. Here the measurement on the  $M$  identical samples can be represented by a collective operator  $\tilde{\mathcal{O}} = \sum_{i=1}^M \mathcal{O}_i$ , where  $\mathcal{O}_i$  denotes the measurement operator acting on the  $i$ th copy. Define the expectation value and variance of the operator  $\mathcal{O}$  in the hypothesis  $\rho_x$  ( $x = 0, 1$ ) by

$$\mu_x = \langle \mathcal{O} \rangle_{\rho_x} \quad \text{and} \quad \sigma_x^2 = \langle \mathcal{O}^2 \rangle_{\rho_x} - \langle \mathcal{O} \rangle_{\rho_x}^2, \quad (5)$$

respectively. Based on the central limit theorem for  $M \gg 1$ , the collective measurement results in a Gaussian-distribution random variable  $\lambda$  with a mean value of  $M\mu_x$  and a variance of  $M\sigma_x^2$  under the hypothesis  $H_x$  ( $x = 0, 1$ ). The decision rule is defined by comparing  $\lambda$  with a threshold  $\lambda_{\text{th}}$ : the hypothesis  $H_0$  is declared when  $\lambda < \lambda_{\text{th}}$  and  $H_1$  otherwise. The performance of the decision-making process is commonly quantified by the error probability [51, 52]

$$P_{\text{err}} = \frac{1}{2}[p(1|0) + p(0|1)], \quad (6)$$

where  $p(1|0)$  represents the false-alarm probability, which is the probability of inferring the presence of the target when it is actually absent. Similarly,  $p(0|1)$  represents the miss probability, which is the probability of inferring the absence of the target when it is actually present. By minimizing the total error probability of Eq. (6) with respect to  $\lambda_{\text{th}}$  and solving for  $\lambda_{\text{th}} = M(\sigma_0\mu_1 + \sigma_1\mu_0) / (\sigma_0 + \sigma_1)$ , we thus obtain the minimum probability of error [9, 15]

$$P_{\text{err}} = \frac{1}{2} \text{erfc} \left( \sqrt{\frac{M}{2}} \text{SNR} \right) < \frac{1}{2} \exp \left[ -\frac{M(\text{SNR})^2}{2} \right], \quad (7)$$

where we have defined the SNR as

$$\text{SNR} \equiv \frac{\mu_1 - \mu_0}{\sigma_1 + \sigma_0}, \quad (8)$$

and the last inequality results from  $\text{erfc}(x) < e^{-x^2/2}$  [52]. From Eq. (7), it indicates that a higher SNR leads to lower probability of error in decision-making process. Hence the problem of finding the best strategy for distinguishing between  $\rho_0$  and  $\rho_1$  is reduced to find the optimal measurement  $\mathcal{O}$  that maximizes the SNR. We shall address the problem of what condition is for the optimal measurement  $\mathcal{O}$  in the following subsection.

### C. Quantum Fisher information

As demonstrated previously, the QI problem can be mapped onto a parameter estimation problem of estimating the reflectivity amplitude  $\eta$  of the object. The performance of estimation is characterized by the mean-square deviation of the unbiased estimator  $\hat{\eta}$  of  $\eta$ . Denoting Eq. (3) by  $\rho_\eta$  (correspondingly  $\rho_{\eta \neq 0} = \rho_1$  and

$\rho_{\eta=0} = \rho_0$ ) and providing the measurement  $\mathcal{O}$  performed on  $\rho_\eta$ , the uncertainty of estimating  $\eta$  is given by the error-propagation formula [48, 53]

$$\Delta^2 \hat{\eta} = \frac{1}{M} \frac{\langle \mathcal{O}^2 \rangle_{\rho_\eta} - \langle \mathcal{O} \rangle_{\rho_\eta}^2}{|\partial_\eta \langle \mathcal{O} \rangle_{\rho_\eta}|^2}, \quad (9)$$

where  $\partial_\eta f \equiv \partial f / \partial \eta$ . The estimation uncertainty was proven to be lower bounded by the quantum Cramér-Rao bound given by

$$\Delta^2 \hat{\eta} \geq (M\mathcal{F})^{-1}, \quad (10)$$

with  $\mathcal{F}$  being the so-called QFI, using the Robertson-Schrödinger uncertainty relation [53]. The bound is saturated when the measurement  $\mathcal{O}$  satisfies the necessary and sufficient condition [53]

$$(\mathcal{O} - \langle \mathcal{O} \rangle_{\rho_\eta}) \sqrt{\rho_\eta} = \alpha L \sqrt{\rho_\eta}, \quad \forall \alpha \in \mathbb{R} \setminus \{0\}, \quad (11)$$

where  $L$  is the Hermitian symmetric logarithmic derivative operator for  $\rho_\eta$  [50, 54, 55].

The crucial step in solving the problem stated in previous section is to establish the relationship between the SNR of Eq. (8) and the uncertainty of Eq. (9). Their relationship can be straightforwardly identified in the limit of  $\eta \rightarrow 1$ . Resorting to the interaction representation associating with  $\mathcal{O}_\eta \equiv U_\eta^\dagger \mathcal{O} U_\eta$ , the expectation value of  $\mathcal{O}$  with respect to the detected state  $\rho_\eta$  can be equivalently expressed as that of  $\mathcal{O}_\eta$  with respect to the initial state  $\rho_{SI} \otimes \rho_B$ , i.e.,  $\langle \mathcal{O} \rangle_{\rho_\eta} = \langle \mathcal{O}_\eta \rangle_{SIB}$ , which can be directly derived as a result of the cyclic property of the trace operation. For small values of  $\eta$ , we approximate the  $\eta$ -dependent operator  $\mathcal{O}_\eta$  as  $\mathcal{O}_\eta \approx \mathcal{O} + \eta [\mathcal{O}, (a_S^\dagger b - a_S b^\dagger)] + o(\eta^2)$  by ignoring higher-order terms in Eq. (1), and then obtain

$$\langle \mathcal{O}_\eta \rangle_{SIB} \approx \langle \mathcal{O} \rangle_{SIB} + \eta \left\langle \left[ \mathcal{O}, (a_S^\dagger b - a_S b^\dagger) \right] \right\rangle_{SIB}. \quad (12)$$

Reminding of the notations  $\rho_{\eta=0} = \rho_0$  and  $\rho_{\eta \neq 0} = \rho_1$ , and the identity  $\langle \mathcal{O} \rangle_{\rho_\eta} = \langle \mathcal{O}_\eta \rangle_{SIB}$ , we can deduce the following two equations in the asymptotic limit  $\eta \rightarrow 0$

$$\mu_1 - \mu_0 = \eta \partial_\eta \langle \mathcal{O} \rangle_{\rho_\eta}, \quad (13)$$

$$\sigma_1^2 = \left( \langle \mathcal{O}^2 \rangle_{\rho_\eta} - \langle \mathcal{O} \rangle_{\rho_\eta}^2 \right) \Big|_{\eta \rightarrow 0} = \sigma_0^2. \quad (14)$$

Here, Eq. (14) tells us that the variances of the measurement operator with respect to the two hypotheses are identical in the limit of  $\eta \rightarrow 0$ . This equality was used in the derivation of Eq. (7) by taking it for granted. Submitting the above two equations into Eq. (8) directly yields

$$\left( \frac{\text{SNR}}{\eta} \right)^2 = \frac{1}{4} \frac{(\partial_\eta \langle \mathcal{O} \rangle_{\rho_\eta})^2}{\langle \mathcal{O}^2 \rangle_{\rho_\eta} - \langle \mathcal{O} \rangle_{\rho_\eta}^2} \Big|_{\eta \rightarrow 0} = \frac{1}{4M\Delta^2 \hat{\eta}}. \quad (15)$$

This is one of key results of this paper as it bridges the two approaches frequently used in the study of QI: state discrimination and parameter estimation. Previously, these approaches were considered separately, and their equivalence relationship was not disclosed. It is evident from Eq. (15) that the SNR of Eq. (8) and the estimation uncertainty of Eq. (9) are completely dependent each other. Consequently, this implies that there is no distinction between target detection and target sensitivity, as defined by Lee *et al.* in Ref. [14].

With Eqs. (10) and (15), we obtain a tight upper bound for the minimum error probability of Eq. (7)

$$P_{\text{err}} < \frac{1}{2} \exp\left(-\frac{\eta^2 M \mathcal{F}}{8}\right). \quad (16)$$

Optimal measurements for saturating this bound can be identified by following the condition of Eq. (11), thereby ensuring the equality  $\text{SNR}/\eta = \sqrt{\mathcal{F}}/2$  holds. The above bound coincides with the bound first derived by Sanz *et al.* in Ref. [22] and alternatively recovered by Noh *et al.* in Ref. [56]. In contrast to these two works, our derivation stems from the equivalence relationship of Eq. (15), thus providing a clear operational meaning of the link between the SNR and the QFI. The bound in terms of the SNR, depicted by Eq. (7), gives the best practically achievable limit on the error probability for a given measurement. On the other hand, the bound in terms of the QFI, depicted by Eq. (16), gives the best theoretically achievable limit on the error probability by using the optimal measurement over all possible measurements. When the two bounds are in agreement, equivalently the condition of  $\text{SNR}/\eta = \sqrt{\mathcal{F}}/2$  satisfies, it implies the measurement of consideration is optimal.

It is worth noting that Eq. (16) is here derived under the assumption that measurements are performed locally. A more lower bound on the error probability could be expected with a global measurement strategy, as predicted by the quantum Chernoff bound [7, 21, 49, 57]. However, implementing such measurements would be a nontrivial task in experiments, despite some efforts being devoted to it [11]. This aspect is beyond the scope of our work.

### III. QUANTUM ILLUMINATION WITH NON-GAUSSIAN STATES

Now, we apply the QFI figure of merit to evaluate the performance of the QI protocols using non-Gaussian states and subsequently identify the optimal measurement for saturating the QFI predicted bound on the error probability by following our derived equivalence condition. The non-Gaussian states of interest here are classified into two groups: MPA-TMSV states and MPS-TMSV states. The MPA-TMSV (or MPS-TMSV) state refers to the resultant state created from the TMSV state by adding (or subtracting) an arbitrary equal number of  $\kappa$  photons to each mode, denoted by  $|\text{TMSV}; +\kappa\rangle_{SI}$  (or

$|\text{TMSV}; -\kappa\rangle_{SI}$ ). Here the multi-photon addition (or subtraction) process can be viewed as a series of successive single-photon addition (or subtraction) operation which can be experimentally realized using a weakly parametric amplifier (or a weakly reflecting beam splitter) [32, 58]. However, the single-photon addition (or subtraction) process is probabilistic. This leads to the success probability of the multi-photon counterpart decreasing exponentially as the number of addition (or subtraction) events increases, which ultimately limits its applicability in practical scenarios. Putting this aside, let us assume the MPA-TMSV and MPS-TMSV states are available for our analysis.

The TMSV state is a linear superposition of Holland-Burnett states [59] and can be expressed by

$$|\text{TMSV}\rangle_{SI} = \sum_{n=0}^{\infty} C_n |n\rangle_S |n\rangle_I, \quad (17)$$

with  $C_n = \sqrt{1-z^2} z^n$ , where  $z = \tanh r$  and  $r$  is the squeezing parameter. It is equipped with equal mean photon numbers on each mode given by  $N_S = N_I = \sinh^2 r$ . The MPA-TMSV and MPS-TMSV states are thus defined as follows

$$|\text{TMSV}; +\kappa\rangle_{SI} = \frac{a_S^{\dagger\kappa} a_I^{\dagger\kappa}}{\sqrt{\mathcal{N}_{\kappa,\kappa}^+}} |\text{TMSV}\rangle_{SI}, \quad (18)$$

$$|\text{TMSV}; -\kappa\rangle_{SI} = \frac{a_S^{\kappa} a_I^{\kappa}}{\sqrt{\mathcal{N}_{\kappa,\kappa}^-}} |\text{TMSV}\rangle_{SI}, \quad (19)$$

where  $\mathcal{N}_{\kappa,\kappa}^{\pm}$  are the corresponding normalization factors, and  $a_I$  is the idler mode. With Eq. (17), they can be rewritten in the following compact form

$$|\text{TMSV}; \pm\kappa\rangle_{SI} = \sum_{n=n_{\pm}}^{\infty} C_n^{(\pm\kappa)} |n \pm \kappa\rangle_S |n \pm \kappa\rangle_I, \quad (20)$$

with  $n_+ = 0$  and  $n_- = \kappa$ , and the notations  $+$  and  $-$  signifying the photon-added case and the photon-subtracted case, respectively. Here the expansion coefficients  $C_n^{(\pm\kappa)}$  are given by [32]

$$C_n^{(+\kappa)} = \frac{z^n \binom{n+\kappa}{\kappa}}{\sqrt{{}_2F_1(\kappa+1, \kappa+1; 1; z^2)}}, \quad (21)$$

$$C_n^{(-\kappa)} = \frac{z^{(n-\kappa)} \binom{n}{\kappa}}{\sqrt{{}_2F_1(\kappa+1, \kappa+1; 1; z^2)}}, \quad (22)$$

where  ${}_2F_1(a, b; c; x)$  is the ordinary hypergeometric function. Obviously, the mean photon numbers of both signal and idler modes for both the MPA-TMSV and MPS-TMSV states are identical and given by (see Appendix A for another form)

$$N_S = N_I = \sum_{n=n_{\pm}}^{\infty} \left[ C_n^{(\pm\kappa)} \right]^2 (n \pm \kappa). \quad (23)$$

We plot in Figs. 2(a) and 2(b) the signal strength using Eq. (23) as a function of  $r$  for both cases. It is evident that both the MPA-TMSV and MPS-TMSV states share two common behaviors: (a) the signal strength increases exponentially as  $r$  increases, and (b) the rate of increase for a given  $\kappa$  becomes pronounced as  $\kappa$  itself increases. The main difference between them is that for the MPA-TMSV states,  $N_S$  starts from a value of  $\kappa$ , whereas for the MPS-TMSV states, it starts from 0. This distinction arises because the TMSV state is equivalent to a twin-vacuum state in the limit of  $r \rightarrow 0$ , and the vacuum state becomes a Fock state under photon addition, while it remains unchanged under photon subtraction. We will observe that this difference significantly affects the performance of MPA-TMSV and MPS-TMSV states in QI tasks.

To evaluate the performance of the aforementioned protocols, we need to compute the QFI for the MPA-TMSV and MPS-TMSV states. With the formula given in [22], the analytical expressions for these QFIs are derived as follows:

$$\mathcal{F}_{\pm\kappa} = \frac{4}{1+N_B} \sum_{n=n_{\pm}+1}^{\infty} \frac{[C_{n-1}^{(\pm\kappa)} C_n^{(\pm\kappa)}]^2 (n \pm \kappa)}{[C_{n-1}^{(\pm\kappa)}]^2 + [C_n^{(\pm\kappa)}]^2 \frac{N_B}{1+N_B}}. \quad (24)$$

It is worth noting that this result is applicable to all states in the form of Eq. (20) since the coefficients  $C_n^{(\pm\kappa)}$  can be arbitrarily set. Notably, for TMSV states ( $\kappa = 0$ ) associating with  $C_n/C_{n-1} = N_S/(N_S + 1)$ , it simplifies to

$$\mathcal{F}_0 = \frac{4N_S}{1+N_B} \frac{1}{1 + \frac{N_S}{1+N_S} \frac{N_B}{1+N_B}}, \quad (25)$$

which was first obtained in [22].

Below, we discuss the attainability of the error probability bounds predicted by Eq. (24) using the measurement  $\mathcal{O} = a_R a_I + a_R^\dagger a_I^\dagger$ , where  $a_R$  represents the reflected mode. This measurement can be realized with linear optical elements and photon counting measurements [9, 22]. In the case of  $\kappa = 0$  (i.e., the TMSV state), it is straightforward to verify that this measurement ensure the equality  $\text{SNR}/\eta = \sqrt{\mathcal{F}_0}/2$  with  $\mu_1 - \mu_0 = 2\eta\sqrt{N_S(1+N_S)}$  and  $\sigma_1^2 = \sigma_0^2 = N_S N_B + (1+N_S)(1+N_B)$ , thus indicating that the measurement  $\mathcal{O}$  is indeed optimal [22]. For the case of  $\kappa \neq 0$ , numerical calculations are employed since solving analytically is challenging. We depict in Figs. 2(c) and 2(d)  $\text{SNR}/\eta$  as a function of  $r$ , with the help of the following results:

$$\mu_1 - \mu_0 = 2\eta \sum_{n=n_{\pm}+1}^{\infty} C_n^{(\pm\kappa)} C_{n-1}^{(\pm\kappa)} (n \pm \kappa), \quad (26)$$

$$\sigma_1^2 = \sigma_0^2 = N_B \sum_{n=n_{\pm}}^{\infty} [C_n^{(\pm\kappa)}]^2 (n \pm \kappa) + (1+N_B) \left\{ 1 + \sum_{n=n_{\pm}}^{\infty} [C_n^{(\pm\kappa)}]^2 (n \pm \kappa) \right\}. \quad (27)$$

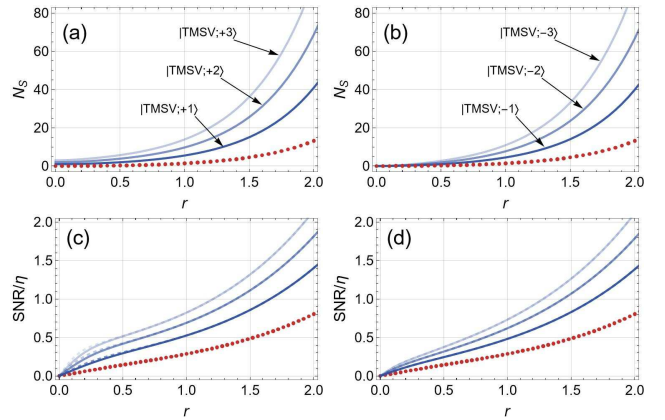


Figure 2. Mean photon number of the signal mode versus the squeezing strength for MPA-TMSV states (a) and MPS-TMSV states (b) with  $N_B = 10$ . In both (a) and (b), the solid lines ranging from darker blue at the bottom to lighter blue at the top correspond to  $|\text{TMSV}; \pm\kappa\rangle_{SI}$  with  $\kappa = 1, 2, 3$ . The red dotted line represents the TMSV state (i.e.,  $\kappa = 0$ ). A comparison between  $\text{SNR}/\eta$  (solid lines) and  $\sqrt{\mathcal{F}_{\pm\kappa}}/2$  (dashed lines) are depicted in (c) and (d) corresponding to the same color schemes used in Figs. 2(a) and 2(b), respectively.

For comparison, we also include the quantity  $\sqrt{\mathcal{F}_{\pm\kappa}}/2$  determined by Eq. (24), in Figs. 2(c) and 2(d) as references. It can be observed that, in the case of MPA-TMSV states, the two quantities,  $\text{SNR}/\eta$  and  $\sqrt{\mathcal{F}_{\pm\kappa}}/2$ , align well for moderately large  $r$ , but display slight difference for small  $r$ . On the other hand, for MPS-TMSV states, they closely coincide across all values of  $r$ . These results indicate that the measurement  $\mathcal{O}$  is globally optimal for MPS-TMSV states, but partially optimal for MPA-TMSV states, depending on  $r$ . Moreover, they have similar trends as the signal strength depicted in Figs. 2(a) and 2(b). The only distinction is that they increases from zero for MPA-TMSV states. From Figs. 2(c) and 2(d), it is evident that both the MPA-TMSV and MPS-TMSV states are superior to the TMSV state when the squeezing strength is constrained. This result is in agreement with the conclusion draw in [46, 47]. However, from another perspective, a contrary conclusion could also be reached.

#### IV. FURTHER DISCUSSIONS

To deeply understand the impact of photon addition and photon subtraction on QI, we engage in further discussions regarding the above scenarios. The aforementioned comparisons are conducted with the assumption the squeezing strength is constrained. These comparisons are unfair as the total energy consumed in these protocols are different. The observed advantages of these non-Gaussian protocols are primarily attributed to the boost in the mean photon number as the number of added or subtracted photons increases, while maintaining the same level of squeezing strength, as shown in Figs. 2(a)

and 2(b). To make a fair comparison, we plot the averaged QFIs  $\mathcal{F}_{\pm\kappa}/N_S$  for both cases as a function of  $r$  in Figs. 3(a) and 3(b). These plots presents completely different trends in comparison to Figs. 2(c) and 2(d), indicating the non-Gaussian states do not outperform the TMSV state. Moreover, the difference between the MPA-TMSV and MPS-TMSV states is evident. In Fig. 3(a), the averaged QFIs start from 0, then reach a plateau around 0.2, and eventually merge with that of the TMSV state. In Fig. 3(b), the averaged QFIs decrease monotonically from 0.36 (corresponding to the value of  $4/(1+N_B)$  with  $N_B=10$ ) to a plateau around 0.2. They also merge with that of the TMSV state at the end. These results indicate that for MPA-TMSV states, there is no advantage when  $r$  is small, and they exhibit comparable performances to the TMSV state as  $r$  modestly increases. In contrast, the MPS-TMSV states perform comparably to the TMSV state when  $r$  approaches 0 or is modestly large, but are poorer elsewhere. Notably, adding or subtracting more photons to the TMSV state can not lead to an increase in the values of the averaged QFIs in comparison against the pictures shown in Fig. 2(c) and 2(d). The sharp difference between these two types of states occurs at  $r \rightarrow 0$ , which arises from the distinct forms of the MPA-TMSV and MPS-TMSV states. Specifically, in the limit of  $r \rightarrow 0$ , the MPA-TMSV state does not have the vacuum state component, whereas the MPS-TMSV state include it.

To better clarify this distinction, let us consider two simple entangled states in the signal-idler mode by

$$|\psi_{-}\rangle_{SI} = \sqrt{1-p}|00\rangle + \sqrt{p}|11\rangle, \quad (28)$$

$$|\psi_{+}\rangle_{SI} = \sqrt{1-p}|11\rangle + \sqrt{p}|22\rangle, \quad (29)$$

where  $p \in [0, 1]$ . Here, the mean photon numbers are  $N_S^- = p$  for  $|\psi_{-}\rangle_{SI}$  and  $N_S^+ = 1 + p$  for  $|\psi_{+}\rangle_{SI}$ . When  $p$  is set to 0, these states represent the MPS-TMSV and MPA-TMSV states in the limit of  $r \rightarrow 0$ , respectively. The QFIs for these states are given by

$$\mathcal{F}_{\pm} = \frac{4x_{\pm}}{1+N_B} \frac{p(1-p)}{(1-p) + p\frac{N_B}{1+N_B}}, \quad (30)$$

where  $x_- = 1$  and  $x_+ = 2$ . The two expressions differ by a constant factor of 2. For the case of  $|\psi_{+}\rangle_{SI}$ , the averaged QFI  $\mathcal{F}_{+}/N_S^+$  equals 0 at  $p = 0$  or 1. It reaches its maximum  $8 \left[ 1 + 3N_B - \sqrt{8(N_B + N_B^2)} \right] / (1 - N_B)^2$  at  $p = \left[ \sqrt{2(N_B + N_B^2)} - N_B \right] / (2 + N_B)$ . In contrast, for the case of  $|\psi_{-}\rangle_{SI}$ , the averaged QFI  $\mathcal{F}_{-}/N_S^-$  reaches its maximum  $4/(1+N_B)$  at  $p = 0$ . These two examples illustrate that Holland-Burnett states are useless for QI, but a state of superposition of the Holland-Burnett states of different photon numbers proves to be useful. Assigning a higher weight to the vacuum state component in the superposition state provides greater advantages for target detection.

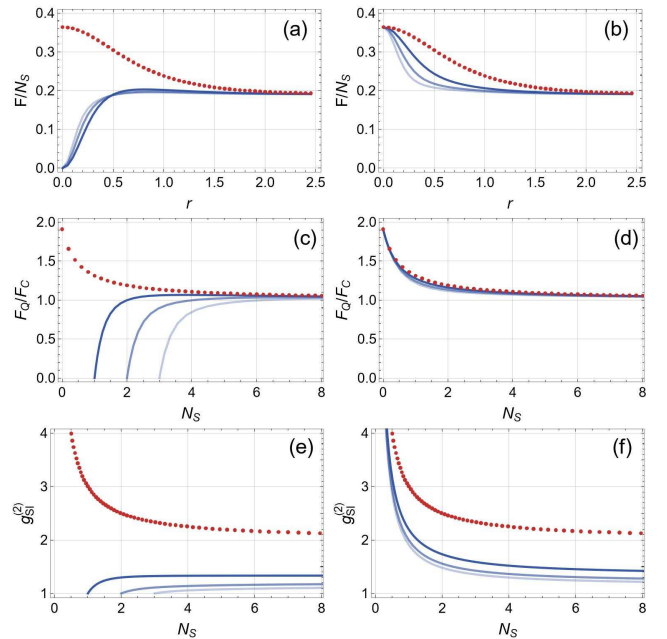


Figure 3. Averaged QFI versus squeezing strength (upper panel), quantum advantage (parameterized by the ratio of quantum QFI to classical QFI) (middle panel) and normalized cross-correlation function (lower panel) versus signal strength for MPA-TMSV states (left column) and MPS-TMSV states (right column) with  $N_B = 10$ . The color schemes employed are consistent with those used in Figs. 2(a) and 2(b).

To evaluate the effects of a QI protocol, the coherent state, which serves as an optimal classical illumination protocol [20], is often used as a benchmark. The QFI for the coherent state is given in [22]

$$\mathcal{F}_c = \frac{4N_S}{1 + 2N_B}, \quad (31)$$

where  $N_S = |\alpha|^2$ , with  $\alpha$  being the amplitude of the coherent state. Here, we adhere to the ratio of  $\mathcal{F}_{\pm\kappa}/\mathcal{F}_c$  defined in [22] to quantify the quantum advantage achievable with the aforementioned non-Gaussian states. In Figs. 3(c) and 3(d), we present plots of this ratio for the MPA-TMSV and MPS-TMSV states as a function of  $N_S$ , considering the coherent state to have the same signal energy as these non-Gaussian states. We observe similar trends consistent with what is shown in Figs. 3(a) and 3(b), indicating that both photon addition and photon subtraction do not confer any advantage when compared to the protocol without their application. As seen in Figs. 3(c) and 3(d), the MPA-TMSV states still prove to be useless for QI. In contrast, the MPS-TMSV states exhibit a slightly lower advantage than the TMSV state, and the differences are almost negligible.

Finally, we provide an insight into the above observed phenomena by examining the normalized cross-

correlation function, defined by [60]

$$g_{SI}^{(2)} \equiv \frac{\langle a_S^\dagger a_S a_I^\dagger a_I \rangle}{\langle a_S^\dagger a_S \rangle \langle a_I^\dagger a_I \rangle}. \quad (32)$$

This function characterizes the intensity correlation between photons in the two distinct modes, a property that can be measured using the Hanbury-Brown and Twiss interferometer method [61]. In our cases, where both modes of the interested states feature symmetric photon statistics ( $\langle a_S^\dagger a_S \rangle = \langle a_I^\dagger a_I \rangle = N_S$ ), thus the expression for Eq. (32) simplifies to  $g_{SI}^{(2)} = \langle a_S^\dagger a_S a_I^\dagger a_I \rangle / N_S^2$ . For the TMSV state, we have  $g_{SI}^{(2)} = 2 + 1/N_S$ . The normalized cross-correlation functions for the MPA-TMSV and MPS-TMSV states are obtained by (see Appendix A for details)

$$g_{SI}^{(2)} = 1 + \frac{\mathcal{N}_{\kappa+1, \kappa+1}^+ \mathcal{N}_{\kappa, \kappa}^+ - (\mathcal{N}_{\kappa+1, \kappa}^+)^2}{(\mathcal{N}_{\kappa+1, \kappa}^+ - \mathcal{N}_{\kappa, \kappa}^+)^2}, \quad (33)$$

and

$$g_{SI}^{(2)} = \frac{\mathcal{N}_{\kappa+1, \kappa+1}^- \mathcal{N}_{\kappa, \kappa}^-}{(\mathcal{N}_{\kappa+1, \kappa}^-)^2}, \quad (34)$$

respectively. Here we introduce the following notations

$$\mathcal{N}_{\kappa, \iota}^+ = (1 - z^2) \sum_{n=0}^{\infty} \frac{z^{2n} (n + \kappa)! (n + \iota)!}{(n!)^2}, \quad (35)$$

and

$$\mathcal{N}_{\kappa, \iota}^- = (1 - z^2) \sum_{n=\kappa}^{\infty} \frac{z^{2n} (n!)^2}{(n - \kappa)! (n - \iota)!}, (\kappa \geq \iota). \quad (36)$$

We plot these results in Figs. 3(e) and 3(f), corresponding to Eqs. (33) and (34), respectively, as a function of  $N_S$ . Interestingly, we observe analogous trends to those depicted in Figs. 3(c) and 3(d), suggesting that both photon addition and photon subtraction do not enhance correlations under the same signal strength. Experimental evidence has been presented to support the above finding in the case of the TMSV state [18]. Therefore, the normalized cross-correlation function would offer valuable insights into understanding which resource matter for the quantum advantage in QI, a topic garnered significant attention [13, 62–64].

## V. CONCLUSION

The two figures of merit: SNR and QFI, arising from state discrimination theory and parameter estimation theory, respectively, establish upper bounds on the minimum error probability in QI tasks when employing local measurement strategies. They were often separately

considered to evaluate the performance of QI protocols, without disclosing their inner connection. In this work, we dealt with this problem by unveiling the equivalence relationship between the SNR and the QFI under the assumption that the reflectivity of the object is low. This relationship not only enriches the theories between state discrimination and parameter estimation but also has a significant operational meaning for identifying optimal measurements in QI tasks.

Furthermore, we applied this equivalence relation to specific cases, exemplifying two QI protocols that use the MPA-TMSV and MPS-TMSV states as input states. By computing the QFI, we determined the upper bounds for these protocols and identifying the optimal measurement needed to reach these bounds. Our results suggested that using photon addition and photon subtraction can not provide a better performance in QI in comparison to without using them. Finally, our study provided an insight that the normalized cross-correlation function may be responsible for the quantum advantage in QI.

## ACKNOWLEDGMENTS

We thank Xiao-Ming Lu for helpful discussions. This work was supported by the NSFC through Grants No. 12005106, the Natural Science Foundation of the Jiangsu Higher Education Institutions of China under Grant No. 20KJB140001 and a project funded by the Priority Academic Program Development of Jiangsu Higher Education Institutions. Y.B.S. acknowledges support from the NSFC through Grants No. 11974189. L.Z. acknowledges support from the NSFC through Grants No. 12175106.

## APPENDIX A: DERIVATION OF NORMALIZED CROSS-CORRELATION FUNCTION FOR THE MPA-TMSV AND MPS-TMSV STATES

In this appendix, we provide a detailed derivation of the normalized cross-correlation function for both the MPA-TMSV and MPS-TMSV states. To facilitate this, we introduce the more general MPA-TMSV and MPS-TMSV states, which allow arbitrary photon additions or subtractions in the signal and idler modes without enforcing equal conditions, represented as [32]

$$|\text{TMSV}; +\kappa, +\iota\rangle_{SI} = \frac{a_S^{\dagger\kappa} a_I^{\dagger\iota}}{\sqrt{\mathcal{N}_{\kappa, \iota}^+}} |\text{TMSV}\rangle_{SI}, \quad (\text{A1})$$

$$|\text{TMSV}; -\kappa, -\iota\rangle_{SI} = \frac{a_S^{\kappa} a_I^{\iota}}{\sqrt{\mathcal{N}_{\kappa, \iota}^-}} |\text{TMSV}\rangle_{SI}, \quad (\text{A2})$$

accompanying with the normalization factors  $\mathcal{N}_{\kappa, \iota}^+$  and  $\mathcal{N}_{\kappa, \iota}^-$ . When assuming  $\kappa = \iota$ , these simplify to the cases in the main text. Here the expressions of these normal-

ization factors are given by [32]

$$\begin{aligned}\mathcal{N}_{\kappa,\ell}^+ &\equiv \langle \text{TMSV} | a_S^\kappa a_I^\ell a_S^\dagger a_I^\dagger | \text{TMSV} \rangle \\ &= (1-z^2) \sum_{n=0}^{\infty} \frac{z^{2n} (n+\kappa)! (n+\ell)!}{(n!)^2},\end{aligned}\quad (\text{A3})$$

and

$$\begin{aligned}\mathcal{N}_{\kappa,\ell}^- &\equiv \langle \text{TMSV} | a_S^\kappa a_I^\ell a_S^\dagger a_I^\dagger | \text{TMSV} \rangle \\ &= (1-z^2) \sum_{n=\kappa}^{\infty} \frac{z^{2n} (n!)^2}{(n-\kappa)! (n-\ell)!}, (\kappa \geq \ell),\end{aligned}\quad (\text{A4})$$

serving as key ingredients for our derivation. During the derivation of the normalized cross-correlation function, the calculation of the following expectations is necessary:  $\langle a_S^\dagger a_S \rangle$ ,  $\langle a_I^\dagger a_I \rangle$  and  $\langle a_S^\dagger a_S a_I^\dagger a_I \rangle$ , where the first two are equal in our considered cases and have already been obtained in Eq. (23). Here, we present an alternative expressions for these expectations in terms of the well-defined normalization factors of Eqs. (A3) and (A4). Let us take  $\langle a_S^\dagger a_S \rangle$  for example. For  $|\text{TMSV}; +\kappa\rangle_{SI}$ , one can directly derive

$$\begin{aligned}\langle a_S^\dagger a_S \rangle &= \frac{1}{\mathcal{N}_{\kappa,\kappa}^+} \langle \text{TMSV} | a_S^\kappa a_I^\ell a_S^\dagger a_S a_S^\dagger a_I^\ell | \text{TMSV} \rangle \\ &= \frac{1}{\mathcal{N}_{\kappa,\kappa}^+} \langle \text{TMSV} | a_S^\kappa (a_S a_S^\dagger - 1) a_S^\dagger a_I^\ell a_I^\dagger | \text{TMSV} \rangle \\ &= \frac{\mathcal{N}_{\kappa+1,\kappa}^+ - \mathcal{N}_{\kappa,\kappa}^+}{\mathcal{N}_{\kappa,\kappa}^+}.\end{aligned}\quad (\text{A5})$$

Following the same procedure used in the preceding derivation, we obtain

$$\langle a_S^\dagger a_S a_I^\dagger a_I \rangle = \frac{\mathcal{N}_{\kappa+1,\kappa+1}^+ - 2\mathcal{N}_{\kappa+1,\kappa}^+ + \mathcal{N}_{\kappa,\kappa}^+}{\mathcal{N}_{\kappa,\kappa}^+}.\quad (\text{A6})$$

Submitting these results into Eq. (32) finally gives Eq. (33). Similarly, for  $|\text{TMSV}; -\kappa\rangle_{SI}$ , we have

$$\langle a_S^\dagger a_S \rangle = \frac{\mathcal{N}_{\kappa+1,\kappa}^-}{\mathcal{N}_{\kappa,\kappa}^-},\quad (\text{A7})$$

$$\langle a_S^\dagger a_S a_I^\dagger a_I \rangle = \frac{\mathcal{N}_{\kappa+1,\kappa+1}^-}{\mathcal{N}_{\kappa,\kappa}^-},\quad (\text{A8})$$

and finally arrive at Eq. (34).

- 
- [1] S. Lloyd, *Science* **321**, 1463 (2008).  
[2] S. Pirandola, B. R. Bardhan, T. Gehring, C. Weedbrook, and S. Lloyd, *Nature Photonics* **12**, 724 (2018).  
[3] J. H. Shapiro, *IEEE Aerospace and Electronic Systems Magazine* **35**, 8 (2020).  
[4] G. Sorelli, N. Treps, F. Grosshans, and F. Boust, *IEEE Aerospace and Electronic Systems Magazine* **37**, 68 (2022).  
[5] M. F. Sacchi, *Phys. Rev. A* **71**, 062340 (2005).  
[6] M. F. Sacchi, *Phys. Rev. A* **72**, 014305 (2005).  
[7] S.-H. Tan, B. I. Erkmen, V. Giovannetti, S. Guha, S. Lloyd, L. Maccone, S. Pirandola, and J. H. Shapiro, *Phys. Rev. Lett.* **101**, 253601 (2008).  
[8] J. H. Shapiro and S. Lloyd, *New Journal of Physics* **11**, 063045 (2009).  
[9] S. Guha and B. I. Erkmen, *Phys. Rev. A* **80**, 052310 (2009).  
[10] S. Barzanjeh, S. Guha, C. Weedbrook, D. Vitali, J. H. Shapiro, and S. Pirandola, *Phys. Rev. Lett.* **114**, 080503 (2015).  
[11] Q. Zhuang, Z. Zhang, and J. H. Shapiro, *Phys. Rev. Lett.* **118**, 040801 (2017).  
[12] Q. Zhuang, Z. Zhang, and J. H. Shapiro, *J. Opt. Soc. Am. B* **34**, 1567 (2017).  
[13] M.-H. Yung, F. Meng, X.-M. Zhang, and M.-J. Zhao, *npj Quantum Information* **6**, 75 (2020).  
[14] S.-Y. Lee, Y. S. Ihn, and Z. Kim, *Phys. Rev. A* **103**, 012411 (2021).  
[15] Y. Jo, S. Lee, Y. S. Ihn, Z. Kim, and S.-Y. Lee, *Phys. Rev. Research* **3**, 013006 (2021).  
[16] E. D. Lopaeva, I. Ruo Berchera, I. P. Degiovanni, S. Olivares, G. Brida, and M. Genovese, *Phys. Rev. Lett.* **110**, 153603 (2013).  
[17] Z. Zhang, S. Mouradian, F. N. C. Wong, and J. H. Shapiro, *Phys. Rev. Lett.* **114**, 110506 (2015).  
[18] D. G. England, B. Balaji, and B. J. Sussman, *Phys. Rev. A* **99**, 023828 (2019).  
[19] F. Xu, X.-M. Zhang, L. Xu, T. Jiang, M.-H. Yung, and L. Zhang, *Phys. Rev. Lett.* **127**, 040504 (2021).  
[20] M. Bradshaw, L. O. Conlon, S. Tserkis, M. Gu, P. K. Lam, and S. M. Assad, *Phys. Rev. A* **103**, 062413 (2021).  
[21] J. Calsamiglia, R. Muñoz Tapia, L. Masanes, A. Acín, and E. Bagan, *Phys. Rev. A* **77**, 032311 (2008).  
[22] M. Sanz, U. Las Heras, J. J. García-Ripoll, E. Solano, and R. Di Candia, *Phys. Rev. Lett.* **118**, 070803 (2017).  
[23] S. Barzanjeh, S. Pirandola, D. Vitali, and J. M. Fink, *Science Advances* **6**, eabb0451 (2020), <https://www.science.org/doi/pdf/10.1126/sciadv.abb0451>.  
[24] M. Dakna, T. Anhut, T. Opatrny, L. Knöll, and D. G. Welsch, *Phys. Rev. A* **55**, 3184 (1997).



- [25] M. Dakna, J. Clausen, L. Knöll, and D. G. Welsch, *Phys. Rev. A* **59**, 1658 (1999).
- [26] J. Wenger, R. Tualle-Brouri, and P. Grangier, *Phys. Rev. Lett.* **92**, 153601 (2004).
- [27] J. Fiurášek, R. García-Patrón, and N. J. Cerf, *Phys. Rev. A* **72**, 033822 (2005).
- [28] A. Kitagawa, M. Takeoka, M. Sasaki, and A. Chefles, *Phys. Rev. A* **73**, 042310 (2006).
- [29] A. Biswas and G. S. Agarwal, *Phys. Rev. A* **75**, 032104 (2007).
- [30] A. Ourjoumtsev, A. Dantan, R. Tualle-Brouri, and P. Grangier, *Phys. Rev. Lett.* **98**, 030502 (2007).
- [31] M. S. Kim, *J. Phys. B: At., Mol. Opt. Phys.* **41**, 133001 (2008).
- [32] C. Navarrete-Benlloch, R. Garcia-Patrón, J. H. Shapiro, and N. J. Cerf, *Phys. Rev. A* **86**, 012328 (2012).
- [33] L. M. Duan, G. Giedke, J. I. Cirac, and P. Zoller, *Phys. Rev. Lett.* **84**, 4002 (2007).
- [34] J. Eisert, D. Browne, S. Scheel, and M. Plenio, *Ann. Phys.* **311**, 431 (2004).
- [35] H. Takahashi, J. S. Neergaard-Nielsen, M. Takeuchi, M. Takeoka, K. Hayasaka, A. Furusawa, and M. Sasaki, *Nature Photonics* **4**, 178 (2010).
- [36] T. Opatrný, G. Kurizki, and D. G. Welsch, *Phys. Rev. A* **61**, 032302 (2000).
- [37] P. T. Cochrane, T. C. Ralph, and G. J. Milburn, *Phys. Rev. A* **65**, 062306 (2002).
- [38] S. Olivares, M. G. A. Paris, and R. Bonifacio, *Phys. Rev. A* **67**, 032314 (2003).
- [39] F. Dell'Anno, S. De Siena, L. Albano, and F. Illuminati, *Phys. Rev. A* **76**, 022301 (2007).
- [40] Y. Yang and F.-L. Li, *Phys. Rev. A* **80**, 022315 (2009).
- [41] F. Dell'Anno, S. De Siena, and F. Illuminati, *Phys. Rev. A* **81**, 012333 (2010).
- [42] R. Birrittella and C. C. Gerry, *J. Opt. Soc. Am. B* **31**, 586 (2014).
- [43] D. Braun, P. Jian, O. Pinel, and N. Treps, *Phys. Rev. A* **90**, 013821 (2014).
- [44] S. Wang, X. X. Xu, Y. J. Xu, and L. J. Zhang, *Opt. Commun.* **444**, 102 (2019).
- [45] W. Zhong, F. Wang, L. Zhou, P. Xu, and Y. B. Sheng, *Sci. China Phys. Mech. Astron.* **63**, 260312 (2020).
- [46] S. Zhang, J. Guo, W. Bao, J. Shi, C. Jin, X. Zou, and G. Guo, *Phys. Rev. A* **89**, 062309 (2014).
- [47] L. Fan and M. S. Zubairy, *Phys. Rev. A* **98**, 012319 (2018).
- [48] B. Yurke, S. L. McCall, and J. R. Klauder, *Phys. Rev. A* **33**, 4033 (1986).
- [49] K. M. R. Audenaert, J. Calsamiglia, R. Muñoz Tapia, E. Bagan, L. Masanes, A. Acín, and F. Verstraete, *Phys. Rev. Lett.* **98**, 160501 (2007).
- [50] S. L. Braunstein and C. M. Caves, *Phys. Rev. Lett.* **72**, 3439 (1994).
- [51] C. Fuchs and J. van de Graaf, *IEEE Transactions on Information Theory* **45**, 1216 (1999).
- [52] H. L. V. Trees, K. L. Bell, and Z. Tian, *Detection, estimation, and filtering theory, Second Edition* (Wiley, 2013).
- [53] W. Zhong, X. M. Lu, X. X. Jing, and X. G. Wang, *J. Phys. A: Math. Theor.* **47**, 385304 (2014).
- [54] C. W. Helstrom, *Quantum Detection and Estimation Theory* (Academic, New York, 1976).
- [55] A. S. Holevo, *Probabilistic and Statistical Aspects of Quantum Theory* (North-Holland, Amsterdam, 1982).
- [56] C. Noh, C. Lee, and S.-Y. Lee, *J. Opt. Soc. Am. B* **39**, 1316 (2022).
- [57] S. Pirandola and S. Lloyd, *Phys. Rev. A* **78**, 012331 (2008).
- [58] S. M. Barnett, G. Ferenczi, C. R. Gilson, and F. C. Speirits, *Phys. Rev. A* **98**, 013809 (2018).
- [59] M. J. Holland and K. Burnett, *Phys. Rev. Lett.* **71**, 1355 (1993).
- [60] R. J. Glauber, *Phys. Rev.* **130**, 2529 (1963).
- [61] R. H. Brown and R. Q. Twiss, *Nature* **177**, 27 (1956).
- [62] C. Weedbrook, S. Pirandola, J. Thompson, V. Vedral, and M. Gu, *New Journal of Physics* **18**, 043027 (2016).
- [63] M. Bradshaw, S. M. Assad, J. Y. Haw, S.-H. Tan, P. K. Lam, and M. Gu, *Phys. Rev. A* **95**, 022333 (2017).
- [64] M. Kim, M.-R. Hwang, E. Jung, and D. Park, *Quantum Information Processing* **22**, 98 (2023).